



Rapid finite-fault analysis of large Mexico earthquakes using teleseismic P waves

C. Mendoza · M. R. Martínez-López

Received: 19 October 2021 / Accepted: 15 February 2022 / Published online: 24 February 2022
© The Author(s), under exclusive licence to Springer Nature B.V. 2022

Abstract We propose a rapid, finite-fault inversion procedure to derive first-order estimates of the coseismic slip following large $M_w > 7$ earthquakes in Mexico using teleseismic P waves obtained in near real time. The procedure uses kinematic fault parameters and waveform properties prescribed based on the magnitude of the event. Two consecutive inversions are performed, one for each of the two nodal planes in the earthquake source mechanism, allowing an automated analysis of the P-wave dataset with minimal manual intervention. Following the inversion process, the appropriate slip model is selected based on seismotectonic considerations in the earthquake source region. The inversion procedure was applied to the Mw 7 Acapulco subduction earthquake of 8 September 2021 using the source parameters posted online by the U.S. Geological Survey (USGS), resulting in the derivation of a preliminary, first-order source model within 1 h after the event. The slip model shows a single source region similar to the rupture area observed by the USGS using body- and surface-wave records. We also conducted a rapid analysis of the teleseismic P waves available for the Mw 8.2 normal-faulting

Chiapas earthquake of 8 September 2017 and recovered a slip model comparable to the finite-fault model obtained by the USGS for that event. For both earthquakes, the time required for waveform retrieval and analysis was less than 5 min, indicating that the procedure can be used to derive timely, preliminary slip models for large Mexico events that would be useful for earthquake early alerting and post-earthquake response.

Keywords Rapid P-wave analysis · Finite-fault source inversion · 2021 Acapulco Mexico earthquake · 2017 Chiapas Mexico earthquake

1 Introduction

It is relatively common to invert globally recorded seismic waves to recover the rupture history of large-magnitude earthquakes. Slip models derived using these data provide images of the spatial and temporal extent of the coseismic rupture that are useful for estimating the expected level of strong ground motion in seismically active areas. Given the need for timely estimates of the coseismic slip in earthquake early alerting and post-earthquake response, several studies have pursued the use of waveform-inversion methodologies to derive the extended properties of the earthquake source in a more rapid manner (e.g., Mendoza 1996; Ji et al. 2004; Dreger et al. 2005; Ammon et al. 2006; Mendoza et al. 2011; Mendoza and Hartzell

C. Mendoza (✉)
Centro de Geociencias, Universidad Nacional Autónoma de México, Querétaro, México 76230
e-mail: mendozac@geociencias.unam.mx

M. R. Martínez-López
Instituto de Geofísica, Universidad Nacional Autónoma de México, Ciudad de México, México 04510

2013; Mendoza 2014). Some seismic-monitoring agencies have incorporated these methodologies in their routine analyses to derive finite-fault models following the occurrence of large, damaging events. An example is the finite-fault slip modeling performed by the U.S. Geological Survey (USGS) using global body- and surface-wave data recorded for large earthquakes (Hayes et al. 2011).

In this study, we propose a finite-fault inversion procedure that uses teleseismic P waves to derive rapid, first-order images of the rupture history for large $M_w > 7$ earthquakes in Mexico. Our motivation is based on the need to derive timely estimates for the extended source properties of large seismic events in a region where this capability has generally been unavailable despite its importance for earthquake early alerting and post-earthquake response. We applied the procedure in near real time to recover a preliminary slip model for the $M_w 7$ earthquake of 8 September 2021 (01:47 UTC) near Acapulco, Guerrero, within 1 h following the event. Additionally, we analyze the teleseismic P waveforms available for the large $M_w 8.2$ normal-faulting Chiapas, Mexico earthquake of 8 September 2017 to examine the performance of the rapid procedure for a large $M_w > 8$ event.

The inversion procedure is based on the iterative finite-fault methodology originally developed by Hartzell and Heaton (1983) and modified by Mendoza and Hartzell (2013) to derive the distribution of coseismic slip in a single inversion. Whereas the iterative process requires multiple inversions to identify the smoothing constraints to impose on the inverse problem, the modified approach uses an internally calculated estimate of the amount of smoothing to derive a preliminary, first-order slip model for the event. Mendoza (2014) used this modified approach to derive a source model for the 20 March 2012 $M_w 7.4$ Ometepec, Mexico earthquake using the shallow, northeast dipping nodal plane from the calculated source mechanism to represent the fault. We extend the methodology presented by Mendoza (2014) to allow two consecutive slip inversions: one for each of the two nodal planes identified in the focal mechanism of the event. The two nodal planes thus define orthogonal faults with different orientation and slip angle buried at a depth consistent with the hypocenter location. The approach allows an automatic application of the inversion procedure that requires minimal manual intervention. The appropriate source model is

selected following the inversion process based on the seismotectonic setting of the earthquake.

2 Teleseismic P-wave data

The rapid analysis procedure uses data records available in near real time from the Incorporated Research Institutes for Seismology (IRIS) Data Management Center (<https://www.iris.edu/hq/>). Vertical, broadband P waveforms recorded by the Global Seismograph Network (GSN) are obtained using the IRIS Perl script FETCHDATA (<https://seiscode.iris.washington.edu/>). The script uses a start time and an end time to define the data interval to be retrieved. We set the start time to the origin time (OT) of the earthquake and the end time to OT +16 min to include P waves recorded within 90° of the epicenter. The retrieved data are in MSEED format, which is then converted to Seismic Analysis Code (SAC) format using the MSEED2SAC code available from IRIS. Station instrument responses are also retrieved with FETCHDATA, and data records are subsequently deconvolved to ground displacement using the SAC analysis package. The ground displacement records are then converted to the binary format used in the inversion, keeping those recorded for stations located between 30° and 90° from the epicenter. Theoretical P arrival times for these stations are calculated with the TauP Toolkit (Crotwell et al. 1999) using the IASP91 reference earth model of Kennett and Engdahl (1991). These arrival times are used to cut the front end of the records to make the start times consistent with those of the synthetics. The records are also resampled to a time step of 1 s and filtered within a prescribed pass-band that depends on the size of the event.

3 Inversion procedure

The finite-fault inversion scheme of Hartzell and Heaton (1983) uses a fault plane of prescribed orientation and dimensions divided into a given number of subfaults. The fault plane is placed at a depth consistent with the hypocenter of the earthquake, and synthetic seismograms are constructed by summing the teleseismic responses of point sources distributed uniformly across each subfault. Figure 1 shows a schematic view of the fault geometry and

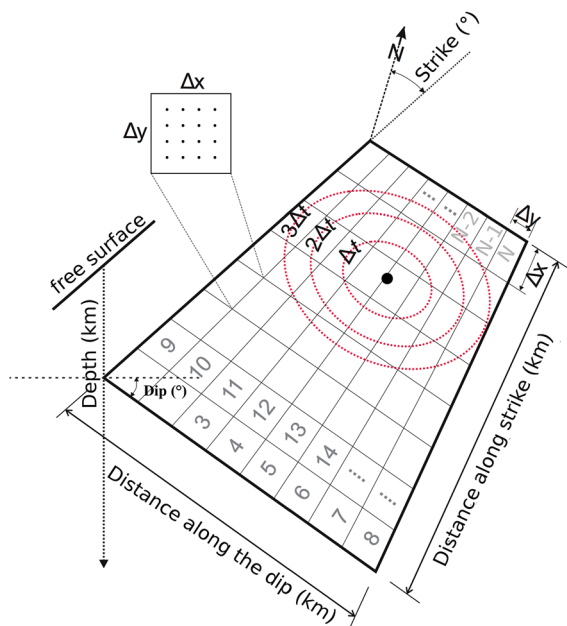


Fig. 1 Spatial parameterization of the fault geometry at depth. The fault is divided into N square subfaults with dimensions $\Delta x = \Delta y$. Point sources distributed across the length and width of each subfault are used to calculate synthetics delayed by Δt times (dotted circles) corresponding to a constant propagation of rupture from the hypocenter (black dot)

parameterization. Point-source responses are calculated for a fixed strike, dip, and rake in a layered near-source crustal structure using generalized ray theory (Helmberger and Harkrider 1978) and include time delays for a constant propagation of rupture away from the hypocenter. We use a three-layer, 35-km crust (Table 1) derived from the gradient velocity model of Stolte et al. (1986) and a rupture velocity of 2.5 km/s. This velocity is ~70% of the shear-wave speed in the crustal structure of Table 1 and corresponds to the rupture propagation speed generally estimated for large earthquakes in Mexico (e.g., Mendoza 1993). A boxcar slip function of fixed width is used to calculate the point-source responses, representing the dislocation duration at any point on the fault, with 100 point sources placed in each subfault to allow for a coherent propagation of rupture.

The synthetics constructed at all the stations for each subfault are placed end-to-end to form the columns of a matrix \mathbf{A} . The observed station records are also placed end-to-end to form a data vector \mathbf{b} . Together, the data and synthetics form an overdetermined system of linear equations $C_d^{-1}\mathbf{A}\mathbf{x}=C_d^{-1}\mathbf{b}$,

where the vector \mathbf{x} contains the amount of slip required in each subfault to reproduce the observations. C_d is a diagonal matrix whose nonzero elements correspond to the peak amplitudes of the data records and is used to normalize the observed waveforms to a peak amplitude of 1.0. The constraints of a fixed dislocation duration and rupture velocity are relaxed by appending additional columns to the coefficient matrix with subfault synthetics successively lagged by the width of the boxcar slip function. The number of columns added denotes the number of time windows used to discretize the rise time on the fault, and the inversion recovers the slip in each subfault for each time window. This identifies longer rise times or delayed slip onsets that may be required by the observations. In this regard, the constant rupture velocity used to delay point-source responses within each subfault corresponds to an upper bound in the inversion.

Constraint equations of the form $\lambda\mathbf{F}\mathbf{x} = 0$ are added to form the linear system

$$\begin{bmatrix} C_d^{-1}\mathbf{A} \\ \lambda_1\mathbf{F}_1 \\ \lambda_2\mathbf{F}_2 \end{bmatrix} \mathbf{x} = \begin{bmatrix} C_d^{-1}\mathbf{b} \\ 0 \\ 0 \end{bmatrix}$$

and a positivity constraint is used to solve for \mathbf{x} . \mathbf{F}_1 incorporates differences in slip between adjacent subfaults, imposing a smooth transition of slip across the fault. \mathbf{F}_2 is the identity matrix, which reduces the length of the solution vector \mathbf{x} and effectively minimizes the total seismic moment. The smoothing parameters λ_1 and λ_2 control the tradeoff between applying the constraints and fitting the observations. In the Hartzell and Heaton (1983) formulation, the same smoothing value ($\lambda_s = \lambda_1 = \lambda_2$) is used in an iterative manner where many inversions are conducted using increasing values of λ_s until the fit between synthetic and observed records becomes visibly degraded. This identifies the simplest solution that fits the observed records. The iterative process, however, is time intensive and difficult to automate. Mendoza (1996) suggested fixing the seismic moment to a known value to constrain the inverse problem and obtain a solution from a single inversion. The approach, however, tends to produce relatively high estimates of the peak slip due to the lack of spatial smoothing across the fault (Mendoza et al. 2011). Mendoza and Hartzell (2013) later examined the inversion process and found an empirical relationship

between the iteratively derived smoothing parameter and the elements of the coefficient matrix $C_d^{-1}\mathbf{A}$. Following an examination of slip models derived using teleseismic P waveforms for different-size events, Mendoza and Hartzell (2013) observed that λ_s can be estimated from

$$\lambda_s \sim 90/N \sum_{i=1}^N |a_i|$$

where $|a_i|$ are the absolute values of the N elements in the coefficient matrix. We use this empirical relation to allow a smooth transition of slip across the fault while simultaneously minimizing the seismic moment. This single-step smoothing process preserves the general character of the extended source and provides a preliminary first-order estimate of the distribution of coseismic slip along the fault (Mendoza and Hartzell 2013).

The rapid procedure is designed to invert P-wave ground-displacement waveforms recorded for $M_w > 7$ earthquakes by adopting input fault parameters that scale with the earthquake size. The subfault size, boxcar duration, and number of time windows are prescribed based on the magnitude of the event and become progressively greater for larger-magnitude events, as suggested by Mendoza and Hartzell (2013). Mendoza and Hartzell (2013) used up to ten time windows with boxcar durations of up to 10s to derive first-order slip models for the April 2012 M_w 8.6 earthquake in Northern Sumatra and the M_w 9.0 Tohoku, Japan earthquake of March 2011. Larger-magnitude events also use a broader frequency content and longer record lengths to allow the recovery of spatial features of the source over larger fault areas (Mendoza and Hartzell 2013). In the application of the inversion procedure, we adopt the scheme presented in Table 2, where input fault parameters and waveform properties are selected automatically based on the size of the earthquake. These prescribed parameters allow an automated analysis of large $M_w > 7$ events that follows the source scaling used by Mendoza and Hartzell (2013) to recover teleseismic slip models for events up to M_w 9.

Prior source information needed to run the procedure includes the hypocenter, the magnitude, and the strike, dip, and rake of the two nodal planes. These source parameters are generally available from earthquake-reporting agencies following an event and

are readily streamed into the inversion procedure. Generally, the hypocenter is placed at the center of the fault. The top edge of the fault, however, is not allowed to extend beyond the free surface. If this occurs, the fault is moved downward along the dip so that the top edge is at a depth of 1 km. Also, the bottom of the fault is not allowed to exceed a depth of 250 km, the limit of the synthetic waveform calculation. If this limit is exceeded, the procedure trims the fault to a narrower width, resulting in a smaller number of subfaults. Upon completion, the procedure generates an azimuthal equidistant map of the stations used in the inversion, plots of the slip models derived for each of the two nodal planes, and plots of the fits between observed and theoretical records. In this study, a DELL Inspiron computer with 8GB RAM and an Intel Core 2.3GHz Processor running a LINUX Ubuntu 20.04 operating system was used to perform the rapid P-wave analyses.

4 The 2021 M_w 7 Acapulco earthquake

We applied the rapid, finite-fault inversion procedure in near real time following the M_w 7 Acapulco earthquake of 8 September 2021 using the source parameters (Table 3) posted online by the USGS within 30 min of the event (<https://earthquake.usgs.gov/earthquakes>). The procedure recovered a total of 26 records in the 30° – 90° distance range from IRIS that were used in the inversion. The total time spent in retrieving the data, processing the observed records, calculating the synthetic waveforms, performing the inversion for both nodal planes, and plotting the results was 3min 16s. Thus, we were able to recover a first-order estimate of the rupture history within an hour following the event.

The procedure uses the earthquake magnitude to assign the fault dimensions, the subfault size, the boxcar duration, the number of time windows, and the record parameters following the specifications given in Table 2. For the M_w 7 Acapulco earthquake, a fault area of $80 \text{ km} \times 80 \text{ km}$ was used in the inversion with the fault divided into 256 square subfaults. A boxcar duration of 1s was used to calculate the subfault synthetics with five time windows that allowed a rise time of up to 5s in the inversion. The teleseismic P waveforms were filtered using a 2–60-s passband and cut to 60-s record lengths.

Figure 2A shows the P-wave slip models obtained in the inversion for nodal planes NP1 and NP2. The shallow, northeast-dipping nodal plane (NP1) is consistent with Cocos-North America plate convergence in the Guerrero portion of the Mexico subduction zone and is identified as the fault plane. The distribution of coseismic slip for NP1 shows a single, relatively simple source similar to the slip area observed in the finite-fault model derived by the USGS using body- and surface-wave records and posted online about 12 h following the

Table 1 Near-source crustal structure used to compute point-source responses in the rapid, finite-fault inversion procedure. Adapted from the gradient velocity model of Stolte et al. (1986)

V _p (km/s)	V _s (km/s)	Thickness (km)
5.8	3.35	6.0
6.4	3.69	19.0
7.0	4.04	10.0
8.0	4.62	-

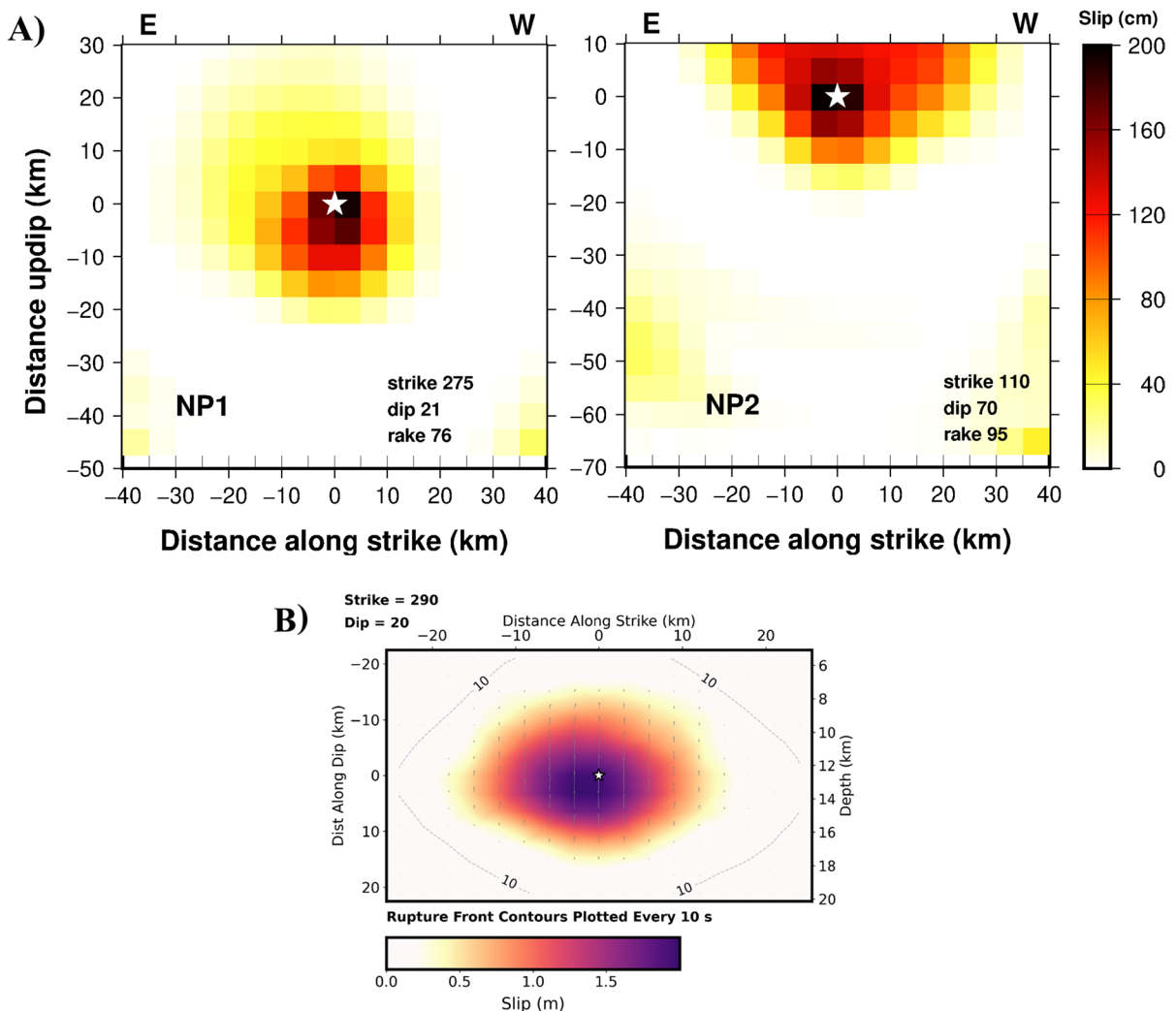


Fig. 2 A Slip model obtained for nodal planes NP1 and NP2 following application of the rapid finite-fault inversion procedure using the teleseismic P waves recorded for the Acapulco earthquake of 8 September 2021. NP1 is identified as the fault plane with a calculated moment of 3.8×10^{26} dyne-cm (Mw

7.0) and a peak slip is 1.9 m. B Finite-fault slip model posted online by the USGS for the event (<https://earthquake.usgs.gov/earthquakes/eventpage/us7000f93v/finite-fault>, accessed 8 september 2021). The hypocenter (star) is at a depth of 12.6 km in all solutions

Table 2 Fault and waveform parameters assigned for different magnitude intervals

Magnitude, M_w	Fault Length (km)	Max Fault Width (km)	Max Number of Subfaults	Subfault Dimension (km ²)	NTW	TWD (s)	Passband Filter (s)	Record Length (s)
$7 \leq M_w < 7.5$	80	80	256	5 x 5	5	1	2-60	60
$7.5 \leq M_w < 8$	120	120	144	10 x 10	5	1	2-80	80
$8 \leq M_w < 8.5$	240	240	144	20 x 20	5	2	2-100	100
$8.5 \leq M_w < 9$	500	300	240	25 x 25	5	5	5-120	120
$M_w \geq 9$	600	300	200	30 x 30	10	10	5-150	150

NTW = number of time windows; TWD = time window duration

Table 3 Source parameters used in the rapid analysis of the teleseismic P waves recorded for the 2021 Acapulco and 2017 Chiapas earthquakes. NP1 and NP2 are the nodal planes identified in the source mechanism of each event

Event	M_w	Origin Time (hr:min:sec)	Hypocenter (Lat/Lon/Depth)	Source Mechanism (Strike/Dip/Rake)
8 Sep 2021 Acapulco ^a	7.0	01:47:46 UTC	16.95°/-99.79°/12.6 km	NP1: 275°/21°/76° NP2: 110°/70°/95°
8 Sep 2017 Chiapas ^b	8.2	04:49:17 UTC	14.76°/-94.10°/45.9 km	NP1: 311°/84°/-95° NP2: 171°/7°/-50°

^a Source parameters from USGS website (<https://earthquake.usgs.gov/earthquakes>)

^b Source parameters from SSN (2017) special report

event (Fig. 2B). The rupture dimensions and peak slips are similar in both solutions, with slip greater than 50cm covering an area of about 25 km × 20 km.

The fits between observed and theoretical records in the rapid P-wave analysis are similar for both nodal planes (Fig. 3), reflecting the general difficulty in using the goodness of fit to distinguish between the causative fault and the auxiliary plane. Euclidean norms $\|Ax-b\|$ obtained for nodal planes NP1 and NP2 are very similar (9.1584 and 9.1756, respectively), indicating that the residual-norm measures are not sufficient to identify the fault plane. The large misfit observed at station TARA, which is at a near-nodal direction for P waves, may be due to errors in the assumed strike of the event given the relatively small peak amplitude of 6.2 microns and the opposite polarity predicted for the P wave. Generally, stations with a large misfit can be disregarded if the majority of the records are well fit. In the case of the 2021 Acapulco earthquake, an independent inversion without the TARA record yields essentially the same result.

5 The 2017 Mw 8.2 Chiapas earthquake

We additionally applied the automated finite-fault inversion procedure to the teleseismic P waves recorded for the Mw 8.2 intraslab earthquake of 8 September 2017 in Chiapas, Mexico. This earthquake resulted from high-angle normal faulting in the downgoing Cocos plate and is the largest event to have occurred in Mexico in the modern instrumental era of Seismology (SSN 2017; Okuwaki and Yagi 2017). The earthquake was widely recorded by modern, digital GSN stations, providing an opportunity to examine the performance of the procedure for a large normal-faulting event. We used the source parameters reported for the event by Mexico's Servicio Sismológico Nacional (SSN 2017) to perform the rapid P-wave analysis (Table 3). The assigned fault area from Table 2 for an event of this size (Mw 8.2) is 240 km × 240 km divided into 144 square subfaults, with five time windows and a 2-s boxcar used to discretize the rise time on the fault. On execution, the procedure identified 39 teleseismic P waveforms filtered within a 2–100-s passband and cut to 100-s record lengths.

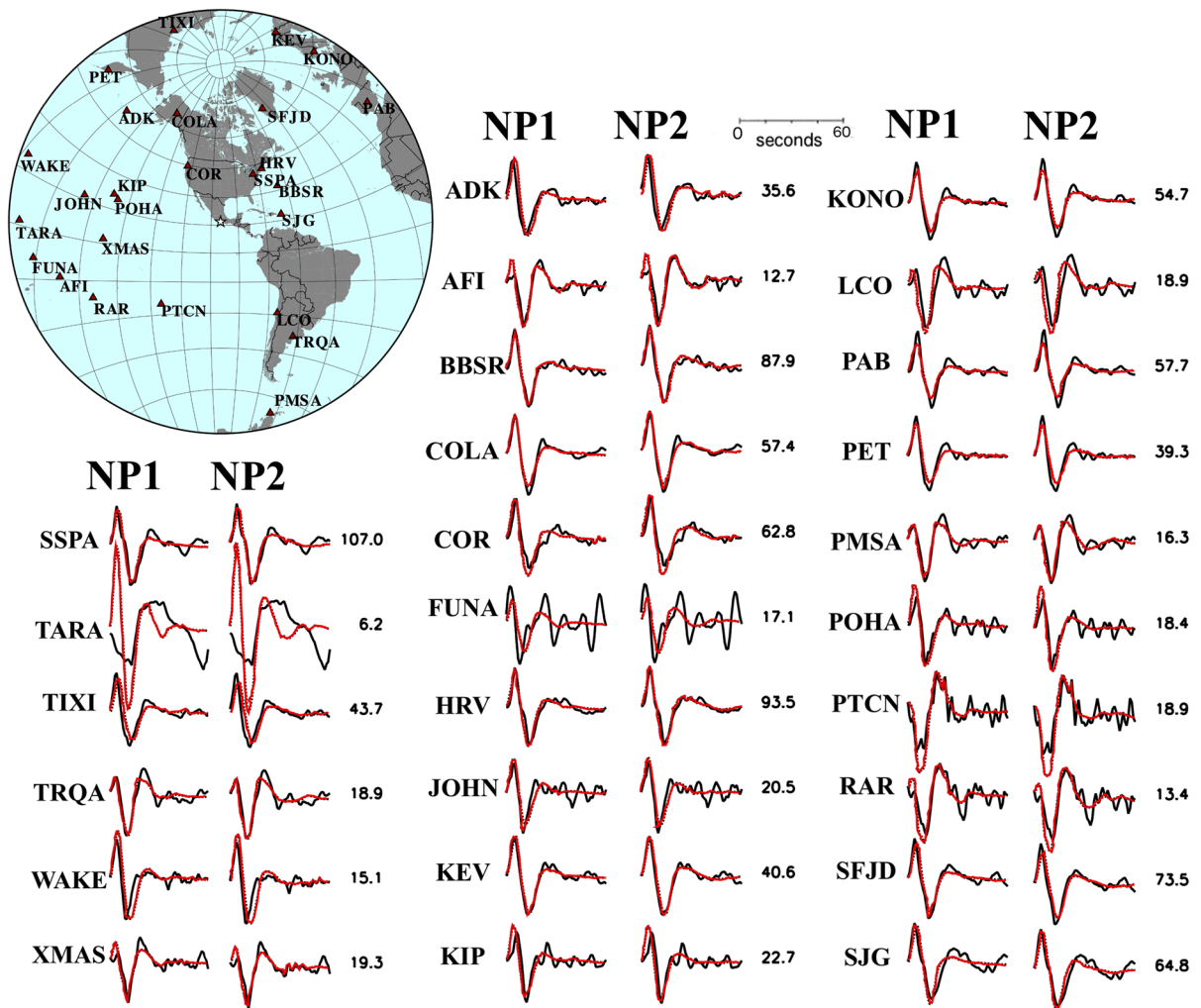


Fig. 3 Azimuthal equidistant projection showing the location of stations used in the rapid analysis of the Mw 7.0 Acapulco earthquake of 8 September 2021 (star). Also shown are the observed P-wave ground-displacement waveforms (black)

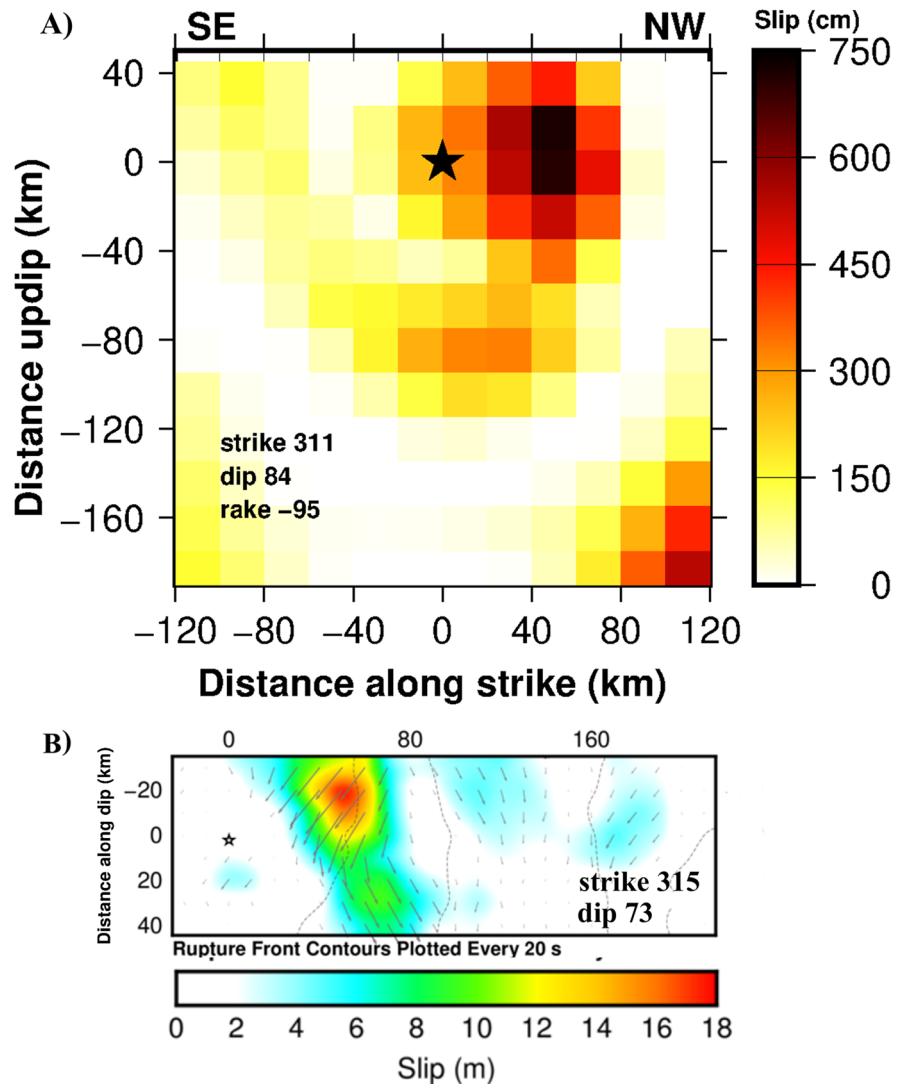
and the predicted records (red) for slip models obtained using nodal planes NP1 and NP2. Numbers to the right of the waveform fits are the peak amplitudes observed at each station (in microns)

The total time elapsed for waveform retrieval and analysis was 2min 30s.

The rupture model obtained for the vertically dipping nodal plane (NP1) is shown in Fig. 4A. This plane has been identified as the causative fault based on seismotectonic considerations (e.g., Okuwaki and Yagi 2017). The finite-fault solution derived by the USGS using a similar fault orientation and hypocenter depth is shown in Fig. 4B. Both solutions show the largest slip to be located 40–60 km northwest of the hypocenter. However, the peak slips in the two solutions differ, with the P-wave model reaching a

maximum of 7.2m compared to ~17m in the USGS model. In a more careful analysis of the teleseismic P waves, Okuwaki and Yagi (2017) also found the principal slip to be located at shallow depths near the hypocenter with a peak slip of ~18m that is more in line with the USGS result. A greater peak slip comparable to the USGS and Okuwaki and Yagi (2017) slip amplitudes could be obtained in the rapid P-wave analysis by using a smaller amount of smoothing in the inversion. This would improve the fit to higher-frequency features observed in the teleseismic P-wave displacements shown in Fig. 5 and would decrease

Fig. 4 **A** Slip model obtained for nodal plane NP1 following application of the rapid finite-fault inversion procedure using the teleseismic P waves recorded for the normal-faulting Chiapas earthquake of 8 September 2017. The peak slip is 7.2 m, and the calculated seismic moment is 3.9×10^{28} dyne-cm (M_w 8.3). **B** Finite-fault slip model derived for the event by the USGS (<https://earthquake.usgs.gov/eventpage/us2000ahv0>, accessed 28 July 2021), shown at the same scale. The hypocenter (star) is at a depth of 45.9 km in the rapid P-wave solution and 47.4 km in the USGS model



the rupture area for the given seismic moment. The observed waveforms, however, are relatively well fit over the longer periods, resulting in a timely estimate of the overall spatial aspects of the source. A closer fit to the observations, in fact, is not warranted given the general assumptions made in the rapid application of the finite-fault inversion methodology.

6 Discussion and conclusions

We describe a rapid finite-fault inversion procedure using teleseismic P waves recorded in near real time to derive a timely, first-order image of the coseismic slip following large $M_w > 7$ earthquakes. The

procedure uses known earthquake source parameters, including the origin time, hypocenter location, and source mechanism to compute slip models using data records downloaded automatically from the Incorporated Research Institutions for Seismology (IRIS) Data Management Center (<http://www.iris.edu>). Input fault dimensions and kinematic rupture parameters are prescribed based on the size of the earthquake to allow flexibility in the rupture velocity and rise time for large events. Two consecutive inversions of the deconvolved ground displacements are performed, one for each of the two nodal planes identified in the earthquake source mechanism. The fits between observed and theoretical records for both nodal planes are similar, and the appropriate slip model is

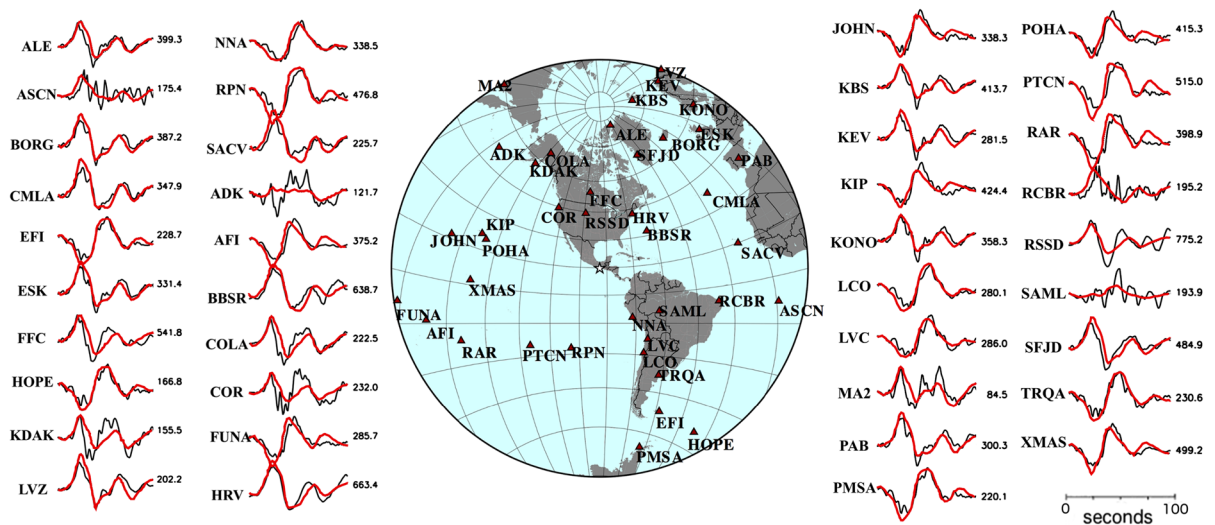


Fig. 5 Station locations and P waveform fits for the Mw 8.2 Chiapas earthquake of 8 September 2017 (star). Observed (black) and predicted (red) ground displacements are shown

for each station. Numbers to the right of the waveform fits are the observed peak amplitudes (in microns)

selected based on seismologic considerations related to the seismotectonic setting of the earthquake source region. For large, shallow subduction earthquakes, for example, the corresponding source model can be readily identified from the orientation and dip of the subducting slab.

Application of the rapid finite-fault analysis procedure to the Mw 7 Acapulco, Mexico subduction earthquake of 8 September 2021 resulted in the derivation of a preliminary, first-order rupture model within an hour following the event. The distribution of coseismic slip derived using the teleseismic P waves shows a single 25 km × 20 km source area that is similar to the rupture model posted online by the USGS about 12 h after the earthquake. We additionally tested the performance of the procedure in an *a posteriori* manner using the teleseismic P waves available from IRIS for the Mw 8.2 normal-faulting earthquake of 8 September 2017 in Chiapas, Mexico. The resulting slip model is also comparable to the source model derived by the USGS, although we obtain a lower peak slip. It is possible to recover additional detail of the source, including higher peak slips, by decreasing the amount of spatial smoothing used in the inversion. This would result in a smaller rupture area and a closer fit to higher-frequency features in the observed records. However, given the general assumptions and

uncertainties associated with the rapid inversion process, improved fits may result in erroneous slip contributions unrelated to the source. For the 2021 Acapulco and 2017 Chiapas earthquakes, the rapid application of the automated inversion procedure to the observed teleseismic P waves recovers the overall spatial features of the source, providing a representative, preliminary estimate of the coseismic slip.

The time elapsed for automatic download of data records and subsequent computation of slip models was less than 5 min for both the Acapulco and Chiapas earthquakes. This excludes the time interval required for locating the earthquake, calculating the magnitude, and deriving the source mechanism. This additional time clearly has to be taken into account in any rapid, near-real-time application since it would dictate how rapidly a preliminary slip model could be derived following the occurrence of an event. For large earthquakes in Mexico, the SSN computes hypocentral locations and regional W-phase mechanisms within 12 min of an event (X. Perez, pers. comm.). Routinely derived SSN source parameters could be readily integrated into the automated inversion procedure proposed here to derive timely, first-order estimates of the coseismic slip that would be useful for rapid alerting and response following the occurrence of large damaging earthquakes in Mexico.

Acknowledgements This work has benefitted from prior collaborative work with S. Hartzell. We thank J. Silva Corona for his assistance in the preparation of Figure 1 and also two anonymous referees whose comments helped improve the presentation of the results.

Declarations

Conflict of interest The authors declare no competing interests.

References

- Ammon CJ, Velasco AA, Lay T (2006) Rapid estimation of first-order rupture characteristics for large earthquakes using surface waves: 2004 Sumatra-Andaman earthquake. *Geophys Res Lett* 33:L14314. <https://doi.org/10.1029/2006GL026303>
- Crotwell HP, Owens TJ, Ritsema J (1999) The TauP toolkit: flexible seismic travel-time and ray-path utilities. *Seism Res Lett* 70:154–160
- Dreger DS, Gee L, Lombard P, Murray MM, Romanowicz B (2005) Rapid finite-source analysis and near-fault strong ground motions: application to the 2003 M_W 6.5 San Simeon and 2004 M_W 6.0 Parkfield earthquakes. *Seism Res Lett* 76:40–48
- Hartzell SH, Heaton TH (1983) Inversion of strong ground motion and teleseismic waveform data for the fault rupture history of the 1979 Imperial Valley, California, earthquake. *Bull Seism Soc Am* 73:1553–1583
- Hayes GP, Earle PS, Benz HM, Wald DJ, Briggs W, and the USGS/NEIC Earthquake Response Team (2011) 88 hours: the U. S. Geological Survey National Earthquake Information Center Response to the 11 March 2011 M_W 9.0 Tohoku Earthquake. *Seism Res Lett* 82:481–493
- Helmberger DV, Harkrider D (1978) Modeling earthquakes with generalized ray theory. In: Miklowitz J, Achenbach JD (eds) *Modern problems in elastic wave propagation*, John Wiley and Sons, New York, pp 499–518
- Ji C, Helmberger DV, Wald DJ (2004) A teleseismic study of the 2002 Denali fault, Alaska, earthquake and implications for rapid strong-motion estimation. *Earthq Spectra* 20:617–637
- Kennett BLN, Engdahl ER (1991) Travel times for global earthquake location and phase identification. *Geophys J Int* 105:429–465
- Mendoza C (1993) Coseismic slip of two large Mexican earthquakes from teleseismic body waveforms: Implications for asperity interaction in the Michoacan plate boundary segment. *J Geophys Res* 98:8197–8210
- Mendoza C (1996) Rapid derivation of rupture history for large earthquakes. *Seism Res Lett* 67:19–26
- Mendoza C (2014) Near-realtime source analysis of the 20 March 2012 Ometepec-Pinotepa Nacional, Mexico earthquake. *Geof Int* 53:211–220
- Mendoza C, Hartzell S (2013) Finite-fault source inversion using teleseismic P waves: Simple parameterization and rapid analysis. *Bull Seism Soc Am* 103:834–844
- Mendoza C, Castro Torres S, Gomez Gonzalez JM (2011) Moment-constrained finite-fault analysis using teleseismic P waves: Mexico subduction zone. *Bull Seism Soc Am* 101:2675–2684
- Okuwaki R, Yagi Y (2017) Rupture process during the M_W 8.1 2017 Chiapas Mexico earthquake: shallow intra-plate normal faulting by slab bending. *Geophys Res Lett* 44:11816–11823. <https://doi.org/10.1002/2017GL075956>
- SSN (2017) Sismo de Tehuantepec (2017-09-07 23:49 M_W 8.2), Reporte especial, Grupo de trabajo del Servicio Sismológico Nacional, Institute of Geophysics, Universidad Nacional Autónoma de Mexico, retrieved 6 July 2021, <http://www.ssn.unam.mx/sismicidad/reportes-especiales/>
- Stolte C, McNally KC, Gonzalez-Ruiz J, Simila GW, Reyes A, Rebollar C, Munguia L, Mendoza L (1986) Fine structure of a post-failure Wadati-Benioff zone. *Geophys Res Lett* 13:577–580

Publisher's note Springer Nature remains neutral with regard to jurisdictional claims in published maps and institutional affiliations.